
Pyramidal Denoising Diffusion Probabilistic Models

Dohoon Ryu¹ Jong Chul Ye^{2,1,3}

¹ Dept. of Bio and Brain Engineering

² Kim Jaechul Graduate School of AI

³ Dept. of Mathematical Sciences

Korea Advanced Institute of Science and Technology (KAIST)

{dh.ryu, jong.ye}@kaist.ac.kr

Abstract

Diffusion models have demonstrated impressive image generation performance, and have been used in various computer vision tasks. Unfortunately, an image generation task using diffusion models is very time-consuming since it requires thousands of sampling steps. To address this problem, here we present a novel pyramidal diffusion model to generate high resolution images starting from much coarser resolution images using a single score function trained with a positional embedding. This enables a time-efficient sampling for image generation, and also solves the low batch size problem when training with limited resources. Furthermore, we show that the proposed approach can be efficiently used for multi-scale super-resolution problem using a single score function.

1 Introduction

Diffusion models produce high quality images via reverse diffusion processes and have achieved impressive performances in many computer vision tasks. Score-based generative models [40] produce images by solving a stochastic differential equation using a score function estimated by a neural network. Denoising diffusion probabilistic model (DDPM) [10, 37] can be considered as discrete form of score-based generative models. Thanks to the state-of-art image generation performance, these diffusion models have been widely investigated for various applications.

For example, the work in [30] trained a diffusion model on the latent space of a convolutional neural network (CNN) based generative model, which enabled various of tasks via cross attention. DiffusionCLIP [17] leveraged contrastive language-image pretraining (CLIP) loss and the denoising diffusion implicit model (DDIM) [38] for text-driven style transfer. ILVR [4] and CCDF [6] proposed conditional diffusion models and their acceleration techniques using unconditionally trained score functions. Also, recently proposed models [26, 29] have achieved incredible performances on text-conditioned image generation and editing.

In spite of the amazing performance and flexible extensions, slow generation speed remains as a critical drawback. To resolve the problem, various approaches have been investigated. Robin et al. and Vahdata et al. [30, 42] trained a diffusion model in a low-dimensional representational space provided by pre-trained autoencoders. DDIM [38] proposed deterministic forward and reverse sampling schemes to accelerate the generation speed. Jing et al. [13] suggested training of an additional score model for sampling in a lower dimensional space. Song et al. [39] proposed a parameterization of covariance term to achieve better performance and faster sampling speed. Jolicoeur et al. [14] used adaptive step size without any tuning and improved classical reverse-diffusion methods. PNDM [23] devised a pseudo numerical method by slightly changing classical numerical methods [34] for speed enhancement. Salimans et al. [33] reduced the sampling time by progressively halving the diffusion step without losing the sample quality. Denoising diffusion GANs [43] enabled large denoising steps through parameterizing the diffusion process by multimodal conditional GANs. For conditional

diffusion, a short forward diffusion steps of corrupted input can reduce the number of reverse diffusion step in SDEdit [25] and RePaint [24], whose theoretical justification was analyzed using the stochastic contraction theory [6].

This paper approaches the slow sampling issue in a different perspective. In contrast to the architecture used in image generation such as GANs, flow-based models [19], and VAE [18] that generates images from low to high resolution via up-convolution, most of the diffusion models adopt UNet-like encoder-decoder architecture where the dimension of inputs and outputs are same. Given this basic characteristics, here we propose a new conditional training method for the score function via positional information, which gives flexibility and speed enhancement in the sampling process of reverse diffusion. Specifically, we develop a multi-scale trainable denoising diffusion probabilistic model by utilizing positional information as a condition for training. Fig. 1 shows the result of generated images in three different resolutions using only one model in the reverse diffusion process, which clearly demonstrates the flexibility of our method. In addition, as a byproduct, we also demonstrate multi-scale super-resolution using a single diffusion model. This is believed to be an important advantage over the existing SR3 [32] or [11], which refines low resolution images to high resolution using cascaded application of multiple diffusion models.

The contribution of this work can be summarized as following:

- We propose a novel method of conditionally training diffusion model for multi-scale image generation by exploiting the positional embedding.
- Using a single score network, we improve the speed of reverse diffusion process in a coarse-to-fine manner while preserving the generation quality and mitigate high computation problem.
- We present multi-scale super resolution which recursively refines the image resolution using a single score model.

2 Background

2.1 Denoising diffusion probabilistic models

In DDPM [10, 37], for a given data distribution $\mathbf{x}_0 \sim q(\mathbf{x}_0)$, we define a forward diffusion process $q(\mathbf{x}_t|\mathbf{x}_{t-1})$ as a Markov chain by gradually adding Gaussian noise at every time steps t , where $\{\beta\}_{t=0}^T$ is a variance schedule:

$$q(\mathbf{x}_T|\mathbf{x}_0) := \prod_{t=1}^T q(\mathbf{x}_t|\mathbf{x}_{t-1}), \quad \text{where} \quad q(\mathbf{x}_t|\mathbf{x}_{t-1}) := \mathcal{N}(\mathbf{x}_t; \sqrt{1-\beta_t}\mathbf{x}_{t-1}, \beta_t\mathbf{I}). \quad (1)$$

With well scheduled $\{\beta\}_{t=0}^T$, the forward process converts a data distribution to an isotropic Gaussian distribution as $t \rightarrow T$. Using the notation $\alpha_t = 1 - \beta_t$ and $\bar{\alpha}_t := \prod_{s=1}^t \alpha_s$, we can sample from $q(\mathbf{x}_t|\mathbf{x}_0)$ in a closed form:

$$\mathbf{x}_t = \sqrt{\bar{\alpha}_t}\mathbf{x}_0 + \sqrt{1-\bar{\alpha}_t}\mathbf{z}, \quad \text{where} \quad \mathbf{z} \sim \mathcal{N}(\mathbf{0}, \mathbf{I}). \quad (2)$$

As the reverse of the forward step $q(\mathbf{x}_{t-1}|\mathbf{x}_t)$ is intractable, DDPM learns parameterized Gaussian transitions $p_\theta(\mathbf{x}_{t-1}|\mathbf{x}_t)$. The reverse process is defined as Markov chain with learned mean and fixed variance, starting from $p(\mathbf{x}_T) = \mathcal{N}(\mathbf{x}_T; \mathbf{0}, \mathbf{I})$:

$$p_\theta(\mathbf{x}_{0:T}) := p_\theta(\mathbf{x}_T) \prod_{t=1}^T p_\theta(\mathbf{x}_{t-1}|\mathbf{x}_t), \quad \text{where} \quad p_\theta(\mathbf{x}_{t-1}|\mathbf{x}_t) := \mathcal{N}(\mathbf{x}_{t-1}; \mu_\theta(\mathbf{x}_t, t), \sigma_t^2\mathbf{I}). \quad (3)$$

where

$$\mu_\theta(\mathbf{x}_t, t) := \frac{1}{\sqrt{\bar{\alpha}_t}} \left(\mathbf{x}_t + (1 - \alpha_t) \mathbf{s}_\theta(\mathbf{x}_t, t) \right), \quad \mathbf{s}_\theta(\mathbf{x}_t, t) = -\frac{1}{\sqrt{1-\bar{\alpha}_t}} \mathbf{z}_\theta(\mathbf{x}_t, t) \quad (4)$$

Here, $\mathbf{s}_\theta(\mathbf{x}_t, t)$ is a score function and $\mathbf{z}_\theta(\mathbf{x}_t, t)$ is trained by optimizing the objective

$$\min_{\theta} L(\theta), \quad \text{where} \quad L(\theta) := \mathbb{E}_{t, \mathbf{x}_0, \mathbf{z}} \left[\|\mathbf{z} - \mathbf{z}_\theta(\sqrt{\bar{\alpha}_t}\mathbf{x}_0 + \sqrt{1-\bar{\alpha}_t}\mathbf{z}, t)\|^2 \right]. \quad (5)$$

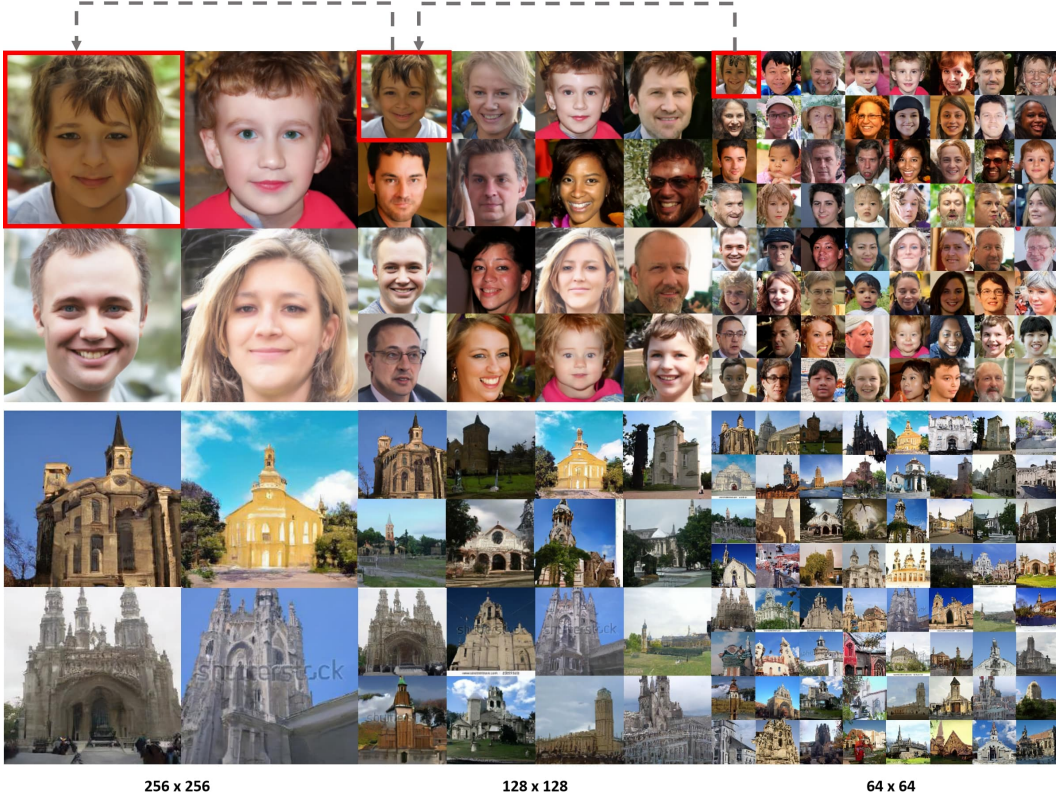


Figure 1: Sampled images of FFHQ [5] and LSUN-Church [44] dataset using the proposed method. Three different resolution images are generated through reverse diffusion processes from a single model. In red boxes, the preservation of the semantic information at different resolution images is observed.

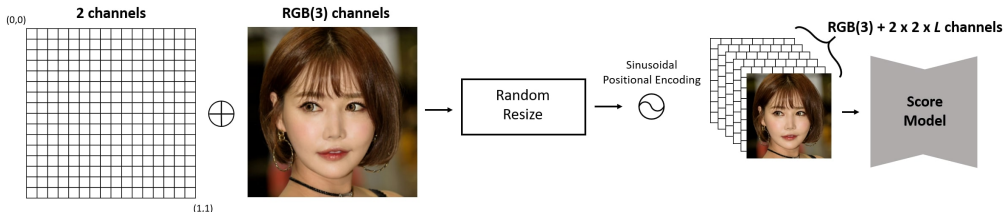


Figure 2: Our training scheme. Two dimensional coordinate information is concatenated with the input image and randomly resized to one of the target resolution. Then, the positional information are encoded with the sinusoidal encoding. Two channels of coordinate values are encoded with the sine and cosine functions, and expanded to $2 \times 2 \times L$ channels where L is the degree of positional encoding.

After the optimization, by plugging learned score function into the generative (or reverse) diffusion process, one can simply sample from $p_\theta(\mathbf{x}_{t-1}|\mathbf{x}_t)$ by

$$\mathbf{x}_{t-1} = \frac{1}{\sqrt{\alpha_t}} \left(\mathbf{x}_t + (1 - \alpha_t) \mathbf{s}_\theta(\mathbf{x}_t, t) \right) + \sigma_t \mathbf{z} \quad (6)$$

2.2 Positional embedding

Positional embedding or encoding are widely used in many recent studies in order to give locational information to deep neural networks. For example, [7, 9] add position embedding to every entry of inputs in the form of trainable parameters. Unlike trainable embedding, [41] proposed a method applying sinusoidal positional encoding of the coordinate values for various tasks such as image

Algorithm 1 Pyramidal reverse diffusion for image generation. It starts from initialization with Gaussian noise at the coarsest resolution, and ends at HR.

Require: $T_f, T_s, \Delta t_s, \{\alpha_t^f\}_{t=1}^{T_f}, \{\alpha_t^s\}_{t=1}^{T_s}, \{\sigma_t^f\}_{t=1}^{T_f}, \{\sigma_t^s\}_{t=1}^{T_s}$

- 1: $\mathbf{x}_{T_f}^{LR} \sim \mathcal{N}(\mathbf{0}, \sigma_{T_f}^f \mathbf{I})$ ▷ Gaussian sampling at the low resolution
- 2: **for** $t = T_f$ to 1 **do** ▷ Full reverse diffusion
- 3: $\mathbf{x}_{t-1}^{LR} \leftarrow \frac{1}{\sqrt{\alpha_t^f}}(\mathbf{x}_t^{LR} + (1 - \alpha_t^f)\mathbf{s}(\mathbf{x}_t^{LR}, t, pos(\mathbf{i}), pos(\mathbf{j})) + \sigma_t^f \mathbf{z})$
- 4: **end for**
- 5: $\mathbf{x}_0 \leftarrow \mathbf{x}_0^{LR}$
- 6: **while** \mathbf{x}_0 is HR **do**
- 7: $\mathbf{x}_0, \mathbf{i}, \mathbf{j} \leftarrow U^{\times 2}(\mathbf{x}_0), U^{\times 2}(\mathbf{i}), U^{\times 2}(\mathbf{j})$ ▷ Upsample image and coordinate value
- 8: $\mathbf{x}_{T_s \Delta t_s} \leftarrow \sqrt{\alpha_{T_s \Delta t_s}^s} \mathbf{x}_0 + \sqrt{1 - \alpha_{T_s \Delta t_s}^s} \mathbf{z}$ ▷ Sample at $T_s \Delta t_s$
- 9: **for** $t = T_s \Delta t_s$ to 1 **do** ▷ Scaled reverse diffusion
- 10: $\mathbf{x}_{t-1} \leftarrow \frac{1}{\sqrt{\alpha_t^s}}(\mathbf{x}_t + (1 - \alpha_t^s)\mathbf{s}(\mathbf{x}_t, t, pos(\mathbf{i}), pos(\mathbf{j})) + \sigma_t^s \mathbf{z})$
- 11: **end for**
- 12: **end while**
- 13: **return** \mathbf{x}_0

regression, 3D shape regression, or MRI reconstruction. As the wave is continuous and periodic, low dimensional information can be expanded to a high dimensional space of different frequencies. In particular, the distance between periodically encoded vectors can be easily calculated by a simple dot product, so that the relative positional information of the data is provided without any additional effort.

The positional information is also useful for training neural network for image generation. Authors in [2] modified StyleGAN2 [16] into a pixel-wise image generation model, which outputs RGB values from the input of 2D coordinate of pixels on image. The models of [45, 36] generate continuous video frame by giving position encoded temporal information to the image generative models. The decoder in [21] generates full images despite the model being only trained with image patches and their center coordinate. Also, [22, 28] train their models through patches and their coordinates, which allows the generative model to bring out arbitrary size of images.

3 Pyramidal Denoising Diffusion Probabilistic Models

In this section, we provide a detailed explanation of our method, called the Pyramidal Denoising Diffusion Probabilistic Models (PDDPM).

Multi-scale score function training Training with multi-scale images is feasible in CNN-based models as they rely on the convolution calculation with spatially invariant filter kernels [1]. Leveraging this simple but strong characteristic of the architecture, our goal is to train diffusion model such that it can understand different scale of the input by giving coordinate information as a condition. Specifically, we concatenate an input image and coordinate values of each pixels (i, j) , while $i, j \in [0, 1]$ are normalized value of its location. Then, random resizing to the target resolution, 64/128/256 in our case, is applied on the merged input. The resized coordinate values are encoded with sinusoidal wave, expanded to high dimensional space, and act as conditions when training as shown in Fig. 2. Specifically, the positional encoding function is given by

$$pos(\gamma) = \left[\sin(2^0 \gamma), \cos(2^0 \gamma), \sin(2^1 \gamma), \cos(2^1 \gamma) \cdots \sin(2^{L-1} \gamma), \cos(2^{L-1} \gamma) \right] \quad (7)$$

$$\gamma = [\gamma_1 \quad \gamma_2 \quad \cdots \quad \gamma_n]^T$$

where $\gamma_i \in [0, 1]$ and L denotes the degree of positional encoding and n is dimension of vector. By denoting $\mathbf{i} = [i_1 \quad i_2 \quad \cdots \quad i_N]^T$, $\mathbf{j} = [j_1 \quad j_2 \quad \cdots \quad j_N]^T$ and N referring to the dimension of \mathbf{x}_t , the training cost function in (5) can be converted as

$$L(\theta) := \mathbb{E}_{t, \mathbf{x}_0, \mathbf{z}} \left[\|\mathbf{z} - \mathbf{z}_\theta(\mathbf{x}_t, t, pos(\mathbf{i}), pos(\mathbf{j}))\|^2 \right]. \quad (8)$$

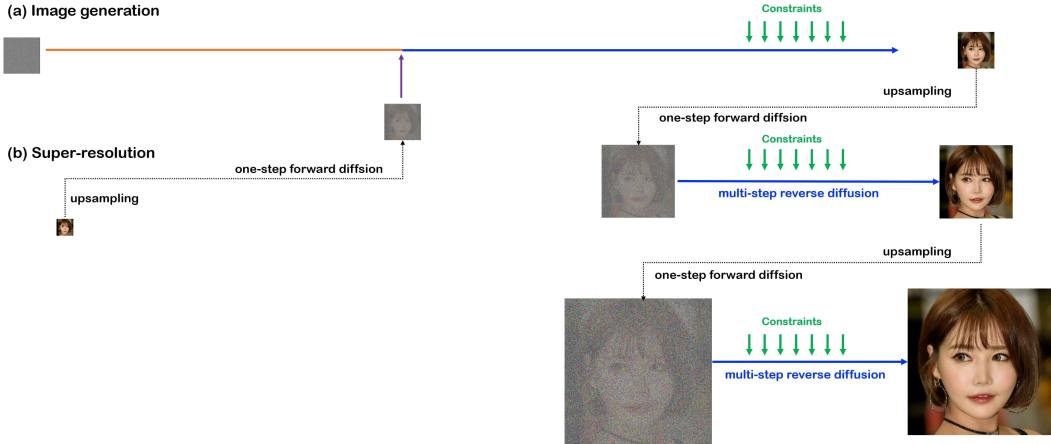


Figure 3: Proposed inference procedure for (a) image generation and (b) super-resolution. At the lowest resolution, full reverse diffusion is performed, which is then upscaled and forward diffused with additional noise. CCDF [6] acceleration scheme is used as an acceleration scheme. For super-resolution, we impose constraints in (10) at every step of the reverse process.

Benefited from the UNet-like model structure [31], the cost function (8) is invariant to all different resolutions so that the optimization can be performed with only a single network. Additionally, a simple idea of scale-free training of the score network significantly improves the network’s flexibility of sampling process which will be discussed later. Importantly, this can also alleviate the problem of slow training and low batch size problems especially when training with limited resources, the latter of which is significant for higher performance generative tasks.

Fast reverse diffusion through pyramidal reverse sampling Thanks to the multi-scale score function, the sampling speed, which is the most critical disadvantage of the diffusion models, can be also made much faster compared to a single full DDPM [38] reverse process. Although one may think our method is similar to [13] which trains additional score network for sampling in lower dimensions, there are several important improvements in our method. First, our method only uses a single score model, which is trained with the positional encoding as explained in (5). Second, inspired by the CCDF acceleration scheme [6], the reverse sampling process can be further accelerated by using the lower-resolution reconstruction as an initialization for the next higher resolution reconstruction.

Specifically, as shown in Algorithm 1 and Fig. 3(a), we first set two different numbers of time steps, T_f and T_s . Here, T_f is a total number of time steps for full reverse diffusion process without any short-cut pass which is applied on generating images of the lowest resolution; T_s is a scaled time step for higher resolution reverse processes for fast sampling. More specifically, starting from low resolution (LR) random Gaussian noise $x_{t=T_f}^{LR} \sim \mathcal{N}(\mathbf{0}, \mathbf{I})$, the full reverse diffusion process is first performed, which is much faster compared to the reverse diffusion process at the maximum resolution. Then the generated LR image and its position values are upsampled twice to produce the initialization for the next resolution. Then, the noises are added to the scaled image through forward diffusion with T_s , after which the reverse diffusion process is performed from $t = T_s \Delta t_s$ to $t = 0$ until the next higher resolution image is generated with $\Delta t_s \in (0, 1)$. This procedure is recursively applied to the next higher resolution images. Using this pyramidal image generation, the total sampling time can be significantly reduced compared to the single-resolution image generation at the highest resolution. According to the CCDF theory [6], the error between the initial estimate and the ground-truth can increase in a polynomial rate during the forward diffusion, whereas the resulting error can be reduced at an exponential rate thanks to the stochastic contraction property of the reverse diffusion. This also implies that the required number of the reverse diffusion can be significantly reduced when a better initialization is used. This explains why we use the previous resolution reconstruction for further acceleration in our method. For theoretical details, see [6].

Pyramidal super resolution with stable gradient guidance Recall that SR3 [32] iteratively refines images from low to high resolution using two different score network modules. Likewise, [11, 29, 39] generate low resolution images, and use one or two different pretrained checkpoints for

Algorithm 2 Pyramidal reverse diffusion for super-resolution. It starts from initialization with input LR image \bar{x}_0 and ends at HR.

Require: $\bar{x}_0, T_s, \Delta t_s, \{\alpha_t^s\}_{t=1}^{T_s}, \{\sigma_t^s\}_{t=1}^{T_s}$

- 1: $\mathbf{x}_0 \leftarrow \bar{x}_0$ ▷ Initialization using LR input image
- 2: **while** \mathbf{x}_0 is *HR* **do**
- 3: $\mathbf{x}_0, \mathbf{i}, \mathbf{j} \leftarrow U^{\times 2}(\mathbf{x}_0), U^{\times 2}(\mathbf{i}), U^{\times 2}(\mathbf{j})$ ▷ Upsample image and coordinate value
- 4: $\mathbf{x}_{T_s \Delta t_s} \leftarrow \sqrt{\bar{\alpha}_{T_s \Delta t_s}^s} \mathbf{x}_0 + \sqrt{1 - \bar{\alpha}_{T_s \Delta t_s}^s} \mathbf{z}$ ▷ Sample at $T_s \Delta t_s$
- 5: **for** $t = T_s \Delta t_s$ to 1 **do** ▷ Scaled reverse diffusion
- 6: $\mathbf{x}_{t-1} \leftarrow \frac{1}{\sqrt{\alpha_t^s}} (\mathbf{x}_t + (1 - \alpha_t^s) \mathbf{s}(\mathbf{x}_t, t, \text{pos}(\mathbf{i}), \text{pos}(\mathbf{j})) + \sigma_t^s \mathbf{z}$
- 7: $\hat{\mathbf{x}}_0(\mathbf{x}_t) := \frac{1}{\sqrt{\bar{\alpha}_t^s}} (\mathbf{x}_t + (1 - \bar{\alpha}_t^s) \mathbf{s}_\theta(\mathbf{x}_t, t, \text{pos}(\mathbf{i}), \text{pos}(\mathbf{j})))$
- 8: $\mathbf{x}_{t-1} \leftarrow \mathbf{x}_{t-1} - \lambda \nabla_{\mathbf{x}_t} \| \mathbf{D} \hat{\mathbf{x}}_0(\mathbf{x}_t) - \bar{x}_0 \|_2^2$
- 9: **end for**
- 10: **end while**
- 11: **return** \mathbf{x}_0

Method	Numerical			DDIM			DDPM			Ours	
	Steps	25	50	100	25	50	100	100	200		1000
FFHQ	30.01	26.03	25.27	29.64	26.49	24.56	16.12	15.23	14.13	15.78	
LSUN-Church*	33.87	28.46	27.15	31.64	29.33	27.59	25.33	24.58	22.11	14.07	
Speed	×22.8	×16.5	×11.1	×40	×20	×10	×10	×5	×1	×10.4	

Table 1: Frechet Inception distance (FID \downarrow) comparison using 10k generated images. Sampling speed was calculated by comparing to full reverse diffusion process. We compared with the pretrained network of [4] for FFHQ. *: A new model is trained from scratch for LSUN-church dataset for fair comparison.

super-resolution. These diffusion models showed impressively high performance, but still requires separately trained networks. However, in our case, only a single model with small number of forward and reverse processes is sufficient as explained in the following and Fig. 3(b).

Specifically, the reverse step can be guided towards the target by subtracting the gradient to the intended direction as suggested in [12, 8, 3]. Specifically, starting from (2), the unconditional prediction of \mathbf{x}_0 given \mathbf{x}_t is first computed by

$$\hat{\mathbf{x}}_0(\mathbf{x}_t) := \frac{1}{\sqrt{\bar{\alpha}_t}} (\mathbf{x}_t + (1 - \bar{\alpha}_t) \mathbf{s}_\theta(\mathbf{x}_t, t, \text{pos}(\mathbf{i}), \text{pos}(\mathbf{j}))) \quad (9)$$

which is mixed with the reverse diffusion samples \mathbf{x}_{t-1} in (6) in terms of additional gradient to update the sample:

$$\mathbf{x}_{t-1} \leftarrow \mathbf{x}_{t-1} - \lambda \nabla_{\mathbf{x}_t} \| \mathbf{D} \hat{\mathbf{x}}_0(\mathbf{x}_t) - \bar{x}_0 \|_2^2 \quad (10)$$

where \mathbf{D} denotes the down-sampling operator and \bar{x}_0 is the low-resolution measurement. Additionally, we use the CCDF acceleration scheme [6] similar to the aforementioned pyramidal image generation. However, one difference from the image generation is that even at the coarsest resolution, the full reverse sampling is not necessary as the lower-resolution measurement can be utilized as an initialization after upsampling. See Algorithm 2 and Fig. 3(b).

4 Experiments

Datasets and Implementation We trained our model using FFHQ 256×256 [5], LSUN-Church 256×256 [44] datasets for 1.2M iterations and 500k for AFHQ-Dog 256×256 dataset with batch size of 48/12/3 for 64/128/256 image resolution. FFHQ and LSUN-Church dataset were used to evaluate generation performances while AFHQ-Dog dataset was used for super-resolution. Our model is based on an improved version of DDPM¹. To alleviate the memory and training speed problem in the

¹<https://github.com/openai/improved-diffusion>

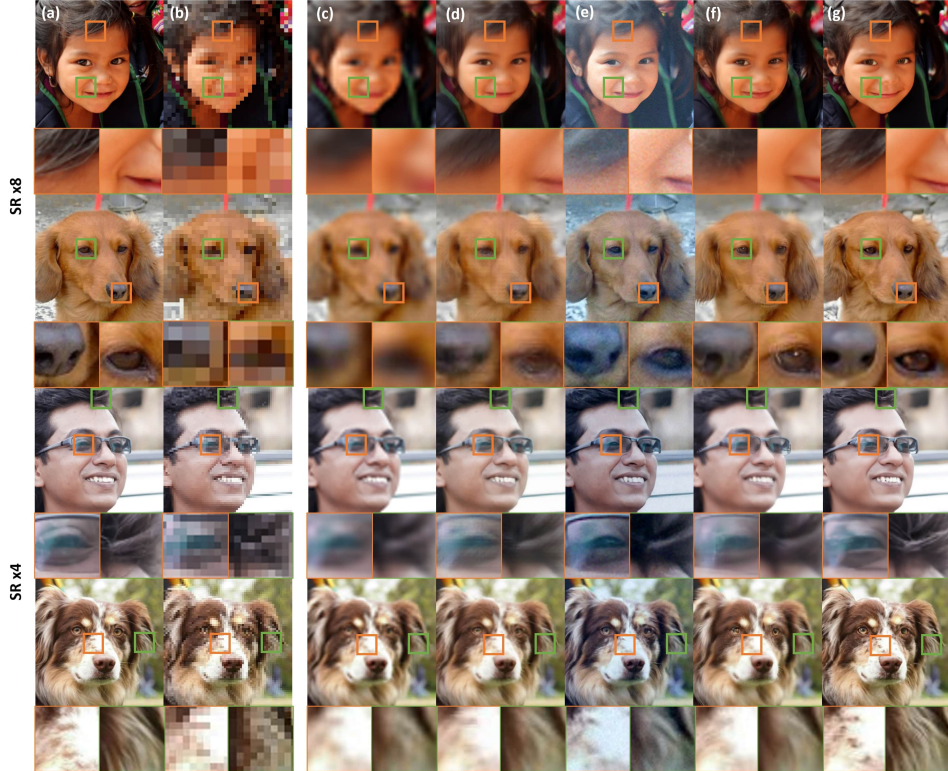


Figure 4: Result of super-resolution on FFHQ and AFHQ-dog dataset. Upper row shows the results of $\times 8$ SR and bottom row is $\times 4$ result. (a) Ground Truth, (b) low resolution images, the results by (c) cubic interpolation, (d) SRGAN, (e) SR3, (f) ILVR, and (g) the proposed method.

limited resource environment using one GeForce 1080 Ti for all model training, we set the number of channels and residual blocks to 64 and 1, respectively, which is a very light model compared to the usual settings. Also we used 1000 diffusion steps for all training. We used Adam optimizer of 0.0001 learning rate. The degree of positional encoding L in (7) was set to 6. For the base setting of the inference, we set $T^f = 1000$ and $T^s = 100$.

Image generation We compared the quality of generated images among different reverse sampling methods. The fourth-order numerical method (linear multi-stepping) [34] is chosen as a classical baseline for reverse diffusion process. For the method, we used Runge-Kutta [34] method for the first three steps for initialization in a similar manner to [23]. We chose 25, 50 and 100 steps for the total sampling steps. DDIM and DDPM methods were also used for the evaluation, and the same steps were performed on DDIM.

For DDPM, above 100 steps were used as it is known to generate reasonable quality images [27]. When sampling from ours, we chose to proceed T^f steps for lowest resolution. For higher resolution, we used T^s steps and $\Delta t_s = 0.3$, so that all samplings procedure of higher resolution images can be done in only 30 steps. The sampling speed was calculated by comparing to the full diffusion step using the same number of parameters and resources setting.

We compared our method with the pre-trained model for FFHQ 256×256 from ILVR repository². The model was trained for 1.2M iterations with batch size of 8 and the number of channels was twice

Δt_s	0.1	0.2	0.3	0.4	0.5
FFHQ	23.91	22.42	22.11	21.91	21.87
LSUN-Church	27.39	18.10	15.38	14.57	14.63
Speed	$\times 59.4$	$\times 38.8$	$\times 26.2$	$\times 21.7$	$\times 18.7$

Table 2: Self-Comparison results. T_f is fixed to 100 which is shorter than the setting in Table 1. FID score and sampling speed are measured in the same way as in Table 1.

²https://github.com/jychoi118/ilvr_adm

SR facotor	FFHQ (256 × 256)								AFHQ (256 × 256)							
	×4				×8				×4				×8			
	Method	FID	LPIPS	PSNR	SSIM	FID	LPIPS	PSNR	SSIM	FID	LPIPS	PSNR	SSIM	FID	LPIPS	PSNR
Bicubic	125.7	0.278	28.84	0.851	151.3	0.446	24.73	0.703	35.34	0.280	<u>29.10</u>	<u>0.816</u>	69.47	0.429	25.34	<u>0.671</u>
SRGAN [20]	46.85	<u>0.204</u>	29.45	<u>0.857</u>	71.69	0.296	26.20	0.753	<u>22.61</u>	0.247	29.48	0.826	45.35	0.329	25.91	0.688
SR3* [32]	59.31	0.291	20.56	0.725	91.57	0.404	18.90	0.612	27.89	0.345	20.15	0.730	<u>35.09</u>	0.401	18.85	0.622
ILVR [4]	54.73	0.224	<u>29.15</u>	0.851	<u>71.47</u>	<u>0.295</u>	<u>24.92</u>	0.712	26.61	0.234	28.76	0.800	37.39	<u>0.326</u>	25.10	0.650
Ours	<u>49.06</u>	0.192	28.70	0.860	66.80	0.289	24.83	<u>0.725</u>	21.62	<u>0.237</u>	27.74	0.796	33.14	0.311	<u>25.38</u>	0.649

Table 3: FID(↓), LPIPS(↓), PSNR(↑), SSIM(↑) score evaluation on super-resolution task. **Bold face**: best, underline: second best. (*:Unofficial re-implementation.)

larger than ours. Despite the small size training data set, our multi-scale training method improved the model by using higher batch size at the lower resolutions. For LSUN-Church 256×256, we trained a new model for 1.2M iterations with equal setting of ours, but with batch size of 4 and without multi-scale ability, for fair comparison. We sampled 10k images from each method and evaluated visual quality using Frechet Inception distance based on `pytorch-fid`³.

The result on FFHQ dataset in Table 1 shows that our method could generate comparable images to the baseline, and even produced higher quantitative metric. Also the result on LSUN-Church dataset confirmed the mitigation of low batch size problem when trained with limited resources. The results shows that the baseline model is not trained sufficiently while ours could carry out the superior result.

We could further speed up the reverse process by re-spacing total diffusion steps of lower dimension also. We changed $T^f = T^s = 100$ and studied the effect of Δt_s on image quality. By fixing total diffusion steps same for all resolution, we compared FID score on generated image when Δt_s value diverged from 0.1 to 0.5. The sampling speed computation was done similar was same as did in Table 1(a). Setting $T^f = 100$ and $\Delta t_s = 0.1$ increased the speed to be 59.4 times faster than original full diffusion process, while generating convincing images. Table 2(b) shows that large sampling steps on high resolution produce higher FID scores, but the sampling speed decreases proportionally to Δt_s . Also, compared to the baselines in Table 1(a), our method produced superior qualitative results despite the faster sampling speed.

Super resolution Experiment was performed on two SR factors: ×4, and ×8. We have tested on FFHQ, AFHQ-Dog 256×256 dataset with our models and other baselines: SRGAN, SR3, ILVR and traditional bicubic upsampling method for comparison. For SRGAN and SR3, there was no checkpoint for appropriate evaluation, so the models were trained on 32→256, 64→256 for each dataset. Additionally, the original work of SR3 [32] cascaded two ×4 upsampler for super-resolution, but in this case we reported on the result of super-resolution with one model for each SR factors. We made a comparison through FID↓, LPIPS↓, PSNR↑ and SSIM↑. Here, LPIPS⁴ was calculated using the open source of the perceptual similarity of VGG [35]. As shown in Table 3, our method produced the best result on FID and LPIPS for most of the cases, but not on PSNR and SSIM. Although SRGAN provides the best PSNR and SSIM values, it contains many image artifacts and the results of our method are more realistic as show in Fig. 4.

Ablation study We performed an ablation study on pyramidal super-resolution and positional encoding. The ablation study on super-resolution was done by removing some steps of the resolution while up-sampling, in order to see the effect of pyramidal super-resolution. For positional encoding, we first trained a new model with multi-scale images without positional encoding. Second, we trained a score model with patches of 256×256 and 512×512 images for generation of 1024×1024 images.

Method	FFHQ		AFHQ	
	FID	LPIPS	FID	LPIPS
32 → 256	72.78	0.308	45.99	0.340
32 → 64 → 256	68.85	0.301	44.25	0.340
32 → 128 → 256	68.33	0.291	36.80	0.328
Original	66.80	0.289	33.14	0.311

Table 4: FID(↓), LPIPS(↓) scores of ablation study on super-resolution tasks.

³<https://github.com/mseitzer/pytorch-fid.git>

⁴<https://github.com/richzhang/PerceptualSimilarity>



Figure 5: Generated images of at full resolution (1024×1024) by our method trained with only 256×256 , 512×512 patches. The model had never seen full resolution image.

Pyramidal super-resolution was evaluated by comparing the original method $32 \rightarrow 64 \rightarrow 128 \rightarrow 256$ with the up-sampling procedures of $32 \rightarrow 64 \rightarrow 256$, $32 \rightarrow 128 \rightarrow 256$ and $32 \rightarrow 256$. The evaluation was performed on both FFHQ and AFHQ-Dog dataset. The result in Table 4 shows that using all the resolution step of pyramidal super-resolution has achieved the best result. The CCDF [6] acceleration scheme of every resolution has shown to improve the quality of reconstructed image.

For the first ablation experiment on the positional encoding, we trained the model with the same experiment setting to the other experiments. It was trained for 800k iterations. Fig. 6 shows the result of the first experiment. Odd looking faces with multiple eyes, crushed face or dislocated facial features were generated. The result confirmed the importance of positional encoding.



Figure 6: Image generated from a multi-scale trained diffusion model without positional encoding. Facial features are not in proper location and some are crushed.

Experiment on patch-wise learning for very high-resolution image generation was performed using one NVIDIA RTX 3090. The model was trained for 400k iterations with batch size of 6/2 on $256/512$ scaled image patches of CelebA-HQ [15] dataset. When training, random resizing and cropping were used. Sampling was performed by setting $T^f = T^s = 100$. As seen in Fig. 5, although the score model had never seen a maximum resolution input, 1024×1024 images were generated through our fast pyramidal image generation.

5 Conclusion

In this work, we proposed a novel Pyramidal DDPM which is trained with conditions on the positional information. We showed that this simple change improves the speed of reverse diffusion process and the performance of super-resolution and image generation. We also tested the effect of positional encoding by additional ablation experiments. Especially, without positional encoding, the model lost the ability to predict proper images at different resolution. Also patch-wise training further improved the flexibility of the score model, generating very high resolution images without using full resolution images. Given the significant advantages from a simple modification, we believe that our method that may further mitigate high computation problem of the diffusion models and be used for many other applications.

Limitations and broader impact While the proposed model accelerates the sampling process, the generative process is still much slower than GANs. For image generation, although our method produced the best in LPIPS and FID, they sometimes lost the original information such as orientation of eyes, shape of teeth or backgrounds. This was because of the generative nature of the diffusion model. As our method highly relies on the generative property of the model, it can be misused for inappropriate purpose such as deepfakes.

References

- [1] Saad Albawi, Tareq Abed Mohammed, and Saad Al-Zawi. Understanding of a convolutional neural network. In *2017 international conference on engineering and technology (ICET)*, pages 1–6. Ieee, 2017.
- [2] Ivan Anokhin, Kirill Demochkin, Taras Khakhulin, Gleb Sterkin, Victor Lempitsky, and Denis Korzhenkov. Image generators with conditionally-independent pixel synthesis. In *Proceedings of the IEEE/CVF Conference on Computer Vision and Pattern Recognition*, pages 14278–14287, 2021.
- [3] Omri Avrahami, Dani Lischinski, and Ohad Fried. Blended diffusion for text-driven editing of natural images. In *Proceedings of the IEEE/CVF Conference on Computer Vision and Pattern Recognition*, pages 18208–18218, 2022.
- [4] Jooyoung Choi, Sungwon Kim, Yonghyun Jeong, Youngjune Gwon, and Sungroh Yoon. ILVR: Conditioning method for denoising diffusion probabilistic models. In *Proceedings of the IEEE/CVF International Conference on Computer Vision (ICCV)*, 2021.
- [5] Yunjey Choi, Youngjung Uh, Jaejun Yoo, and Jung-Woo Ha. Stargan v2: Diverse image synthesis for multiple domains. In *Proceedings of the IEEE/CVF conference on computer vision and pattern recognition*, pages 8188–8197, 2020.
- [6] Hyungjin Chung, Byeongsu Sim, and Jong Chul Ye. Come-closer-diffuse-faster: Accelerating conditional diffusion models for inverse problems through stochastic contraction. *arXiv preprint arXiv:2112.05146*, 2021.
- [7] Jacob Devlin, Ming-Wei Chang, Kenton Lee, and Kristina Toutanova. Bert: Pre-training of deep bidirectional transformers for language understanding. *arXiv preprint arXiv:1810.04805*, 2018.
- [8] Prafulla Dhariwal and Alexander Quinn Nichol. Diffusion models beat GANs on image synthesis. In A. Beygelzimer, Y. Dauphin, P. Liang, and J. Wortman Vaughan, editors, *Advances in Neural Information Processing Systems*, 2021.
- [9] Alexey Dosovitskiy, Lucas Beyer, Alexander Kolesnikov, Dirk Weissenborn, Xiaohua Zhai, Thomas Unterthiner, Mostafa Dehghani, Matthias Minderer, Georg Heigold, Sylvain Gelly, et al. An image is worth 16x16 words: Transformers for image recognition at scale. *arXiv preprint arXiv:2010.11929*, 2020.
- [10] Jonathan Ho, Ajay Jain, and Pieter Abbeel. Denoising diffusion probabilistic models. In *Advances in Neural Information Processing Systems*, volume 33, pages 6840–6851, 2020.
- [11] Jonathan Ho, Chitwan Saharia, William Chan, David J Fleet, Mohammad Norouzi, and Tim Salimans. Cascaded diffusion models for high fidelity image generation. *Journal of Machine Learning Research*, 23(47):1–33, 2022.
- [12] Jonathan Ho, Tim Salimans, Alexey Gritsenko, William Chan, Mohammad Norouzi, and David J Fleet. Video diffusion models. *arXiv preprint arXiv:2204.03458*, 2022.
- [13] Bowen Jing, Gabriele Corso, Renato Berlinghieri, and Tommi Jaakkola. Subspace diffusion generative models. *arXiv preprint arXiv:2205.01490*, 2022.
- [14] Alexia Jolicoeur-Martineau, Ke Li, Rémi Piché-Taillefer, Tal Kachman, and Ioannis Mitliagkas. Gotta go fast when generating data with score-based models. *arXiv preprint arXiv:2105.14080*, 2021.
- [15] Tero Karras, Timo Aila, Samuli Laine, and Jaakko Lehtinen. Progressive growing of gans for improved quality, stability, and variation. *arXiv preprint arXiv:1710.10196*, 2017.
- [16] Tero Karras, Samuli Laine, Miika Aittala, Janne Hellsten, Jaakko Lehtinen, and Timo Aila. Analyzing and improving the image quality of stylegan. In *Proceedings of the IEEE/CVF conference on computer vision and pattern recognition*, pages 8110–8119, 2020.

- [17] Gwanghyun Kim and Jong Chul Ye. Diffusionclip: Text-guided image manipulation using diffusion models. *arXiv preprint arXiv:2110.02711*, 2021.
- [18] Diederik P Kingma and Max Welling. Auto-encoding variational bayes. *arXiv preprint arXiv:1312.6114*, 2013.
- [19] Durk P Kingma and Prafulla Dhariwal. Glow: Generative flow with invertible 1x1 convolutions. *Advances in neural information processing systems*, 31, 2018.
- [20] Christian Ledig, Lucas Theis, Ferenc Huszár, Jose Caballero, Andrew Cunningham, Alejandro Acosta, Andrew Aitken, Alykhan Tejani, Johannes Totz, Zehan Wang, et al. Photo-realistic single image super-resolution using a generative adversarial network. In *Proceedings of the IEEE conference on computer vision and pattern recognition*, pages 4681–4690, 2017.
- [21] Chieh Hubert Lin, Chia-Che Chang, Yu-Sheng Chen, Da-Cheng Juan, Wei Wei, and Hwann-Tzong Chen. Coco-gan: Generation by parts via conditional coordinating. In *Proceedings of the IEEE/CVF international conference on computer vision*, pages 4512–4521, 2019.
- [22] Chieh Hubert Lin, Hsin-Ying Lee, Yen-Chi Cheng, Sergey Tulyakov, and Ming-Hsuan Yang. Infinitygan: Towards infinite-resolution image synthesis. *arXiv e-prints*, pages arXiv–2104, 2021.
- [23] Luping Liu, Yi Ren, Zhijie Lin, and Zhou Zhao. Pseudo numerical methods for diffusion models on manifolds. *arXiv preprint arXiv:2202.09778*, 2022.
- [24] Andreas Lugmayr, Martin Danelljan, Andres Romero, Fisher Yu, Radu Timofte, and Luc Van Gool. Repaint: Inpainting using denoising diffusion probabilistic models. *arXiv preprint arXiv:2201.09865*, 2022.
- [25] Chenlin Meng, Yang Song, Jiaming Song, Jiajun Wu, Jun-Yan Zhu, and Stefano Ermon. SDEdit: Image synthesis and editing with stochastic differential equations. *arXiv preprint arXiv:2108.01073*, 2021.
- [26] Alex Nichol, Prafulla Dhariwal, Aditya Ramesh, Pranav Shyam, Pamela Mishkin, Bob McGrew, Ilya Sutskever, and Mark Chen. Glide: Towards photorealistic image generation and editing with text-guided diffusion models. *arXiv preprint arXiv:2112.10741*, 2021.
- [27] Alexander Quinn Nichol and Prafulla Dhariwal. Improved denoising diffusion probabilistic models. In *International Conference on Machine Learning*, pages 8162–8171. PMLR, 2021.
- [28] Evangelos Ntavelis, Mohamad Shahbazi, Iason Kastanis, Radu Timofte, Martin Danelljan, and Luc Van Gool. Arbitrary-scale image synthesis. *arXiv preprint arXiv:2204.02273*, 2022.
- [29] Aditya Ramesh, Prafulla Dhariwal, Alex Nichol, Casey Chu, and Mark Chen. Hierarchical text-conditional image generation with clip latents. *arXiv preprint arXiv:2204.06125*, 2022.
- [30] Robin Rombach, Andreas Blattmann, Dominik Lorenz, Patrick Esser, and Björn Ommer. High-resolution image synthesis with latent diffusion models. *arXiv preprint arXiv:2112.10752*, 2021.
- [31] Olaf Ronneberger, Philipp Fischer, and Thomas Brox. U-net: Convolutional networks for biomedical image segmentation. In *International Conference on Medical image computing and computer-assisted intervention*, pages 234–241. Springer, 2015.
- [32] Chitwan Saharia, Jonathan Ho, William Chan, Tim Salimans, David J Fleet, and Mohammad Norouzi. Image super-resolution via iterative refinement. *arXiv preprint arXiv:2104.07636*, 2021.
- [33] Tim Salimans and Jonathan Ho. Progressive distillation for fast sampling of diffusion models. *arXiv preprint arXiv:2202.00512*, 2022.
- [34] Timothy Sauer. *Numerical analysis*. Addison-Wesley Publishing Company, 2011.
- [35] Karen Simonyan and Andrew Zisserman. Very deep convolutional networks for large-scale image recognition. *arXiv preprint arXiv:1409.1556*, 2014.

- [36] Ivan Skorokhodov, Sergey Tulyakov, and Mohamed Elhoseiny. Stylegan-v: A continuous video generator with the price, image quality and perks of stylegan2. *arXiv preprint arXiv:2112.14683*, 2021.
- [37] Jascha Sohl-Dickstein, Eric Weiss, Niru Maheswaranathan, and Surya Ganguli. Deep unsupervised learning using nonequilibrium thermodynamics. In *International Conference on Machine Learning*, pages 2256–2265. PMLR, 2015.
- [38] Jiaming Song, Chenlin Meng, and Stefano Ermon. Denoising diffusion implicit models. In *9th International Conference on Learning Representations, ICLR*, 2021.
- [39] Yang Song and Stefano Ermon. Improved techniques for training score-based generative models. In *Advances in Neural Information Processing Systems*, volume 33, pages 12438–12448, 2020.
- [40] Yang Song, Jascha Sohl-Dickstein, Diederik P. Kingma, Abhishek Kumar, Stefano Ermon, and Ben Poole. Score-based generative modeling through stochastic differential equations. In *9th International Conference on Learning Representations, ICLR*, 2021.
- [41] Matthew Tancik, Pratul Srinivasan, Ben Mildenhall, Sara Fridovich-Keil, Nithin Raghavan, Utkarsh Singhal, Ravi Ramamoorthi, Jonathan Barron, and Ren Ng. Fourier features let networks learn high frequency functions in low dimensional domains. *Advances in Neural Information Processing Systems*, 33:7537–7547, 2020.
- [42] Arash Vahdat, Karsten Kreis, and Jan Kautz. Score-based generative modeling in latent space. *Advances in Neural Information Processing Systems*, 34:11287–11302, 2021.
- [43] Zhisheng Xiao, Karsten Kreis, and Arash Vahdat. Tackling the generative learning trilemma with denoising diffusion gans. *arXiv preprint arXiv:2112.07804*, 2021.
- [44] Fisher Yu, Yinda Zhang, Shuran Song, Ari Seff, and Jianxiong Xiao. Lsun: Construction of a large-scale image dataset using deep learning with humans in the loop. *arXiv preprint arXiv:1506.03365*, 2015.
- [45] Sihyun Yu, Jihoon Tack, Sangwoo Mo, Hyunsu Kim, Junho Kim, Jung-Woo Ha, and Jinwoo Shin. Generating videos with dynamics-aware implicit generative adversarial networks. *arXiv preprint arXiv:2202.10571*, 2022.

A Additional results

A.1 Additional samples

In this section, we provide additional samples of different resolution generated from a single score model on FFHQ and LSUN-Church dataset in Fig. 7 and Fig. 8.

A.2 Super-resolution: Intermediate results

In this section, we provide intermediate results on pyramidal super-resolution task. Fig. 9 shows up-scaled images of each resolution starting from 32×32 on FFHQ and AFHQ-dog dataset.

A.3 Super-resolution: Self-comparison results

We visualized the result in Table. 4 in Fig. 10 and Fig. 11. Both of the result show that direct path from the low resolution image to the maximum resolution produce odd-looking details in the images. This implies the effect of iterative refinement method is not trivial.

B Experimental details

B.1 Comparison methods

B.1.1 Image generation

DDIM We used the score function from ILVR [4] repository⁵ as a baseline for FFHQ dataset. The model uses convolution channels starting from 128 which is twice larger than ours. It was trained for 1M iterations with batch size of 8. For LSUN-Church dataset, we trained a new score function of number of channels starting from 64 and 1 residual block with batch size of 4. The setting was equal to our network, but without multi-scale property. The images were generated from DDIM steps of 25 and 50. We used one GeForce 1080 Ti for training.

DDPM We used the same score function of DDIM method. The images were generated from DDPM steps of 100 and 200.

B.1.2 Super resolution

SRGAN We trained a model from scratch on FFHQ and AFHQ-dog dataset using a code from SRGAN repository⁶. The model was trained for 500k iteration for each dataset. The model was trained with batch size of 8, 0.001 learning rate, $0.9 \beta_1$ and $0.999 \beta_2$ using Adam optimizer. We used one GeForce 1080 Ti for training.

SR3 We used unofficial implementation for SR3 model from github repository⁷. The official model trained two separate model for $\times 4$ super-resolution, but we trained a single upsampler for $32 \rightarrow 256$ and $64 \rightarrow 256$. The training was done for 500k iteration with batch size of 2 for each dataset. The model consists of inner channels starting from 64 and 2 residual blocks. It was trained with 0.0001 learning rate using Adam optimizer. We used one GeForce 1080 Ti for training.

ILVR We used pretrained network for both dataset from ILVR repository⁸. It was trained for 1M iterations for FFHQ, and 500k for AFHQ-dog. The model architecture and training setting were same as the one we used for DDIM and DDPM sampling.

⁵https://github.com/jychoi118/ilvr_adm

⁶<https://github.com/leftthomas/SRGAN>

⁷<https://github.com/Janspiry/Image-Super-Resolution-via-Iterative-Refinement>

⁸https://github.com/jychoi118/ilvr_adm

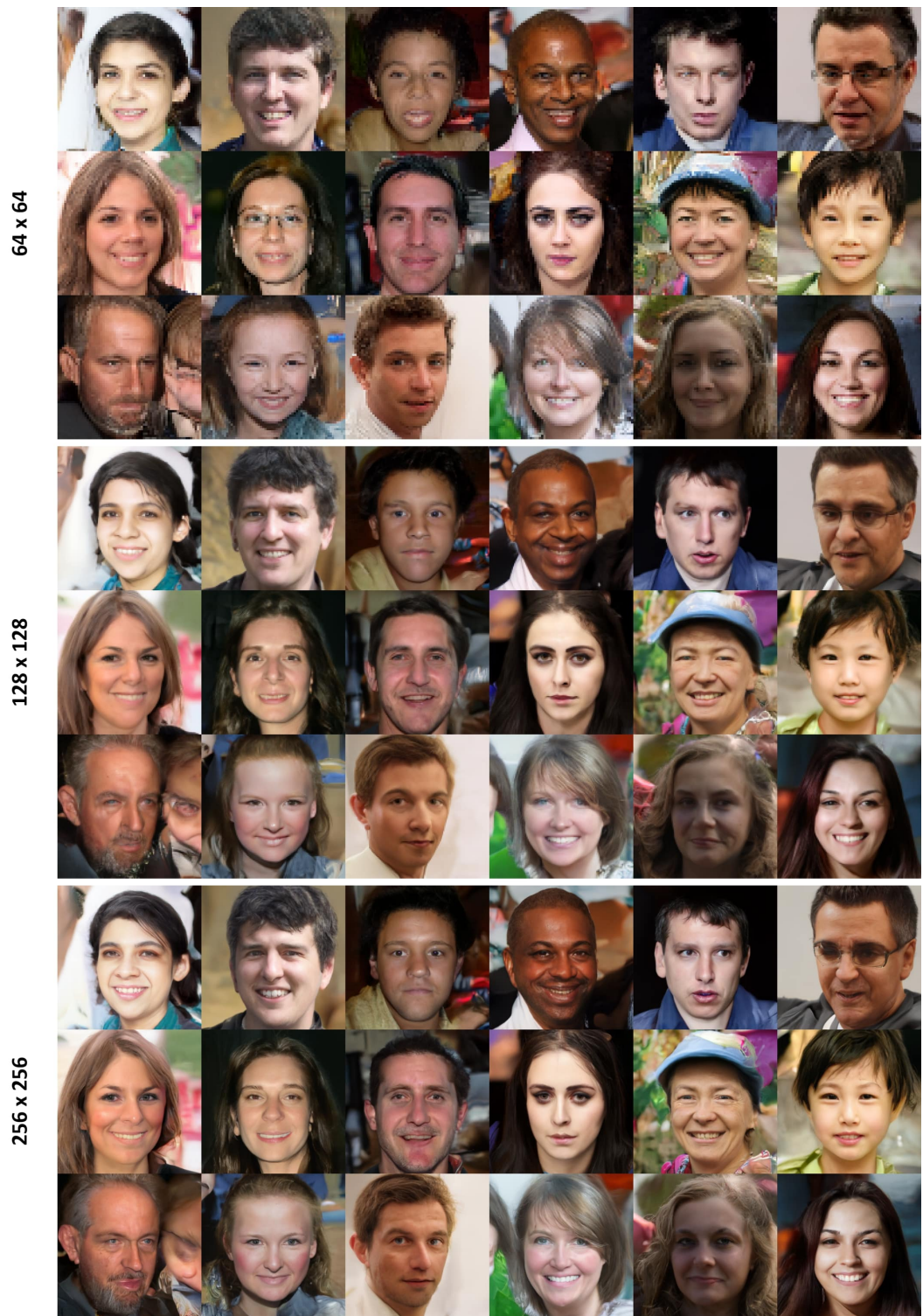


Figure 7: Additional generated images trained from FFHQ dataset. Resolution increases starting from top to bottom row.

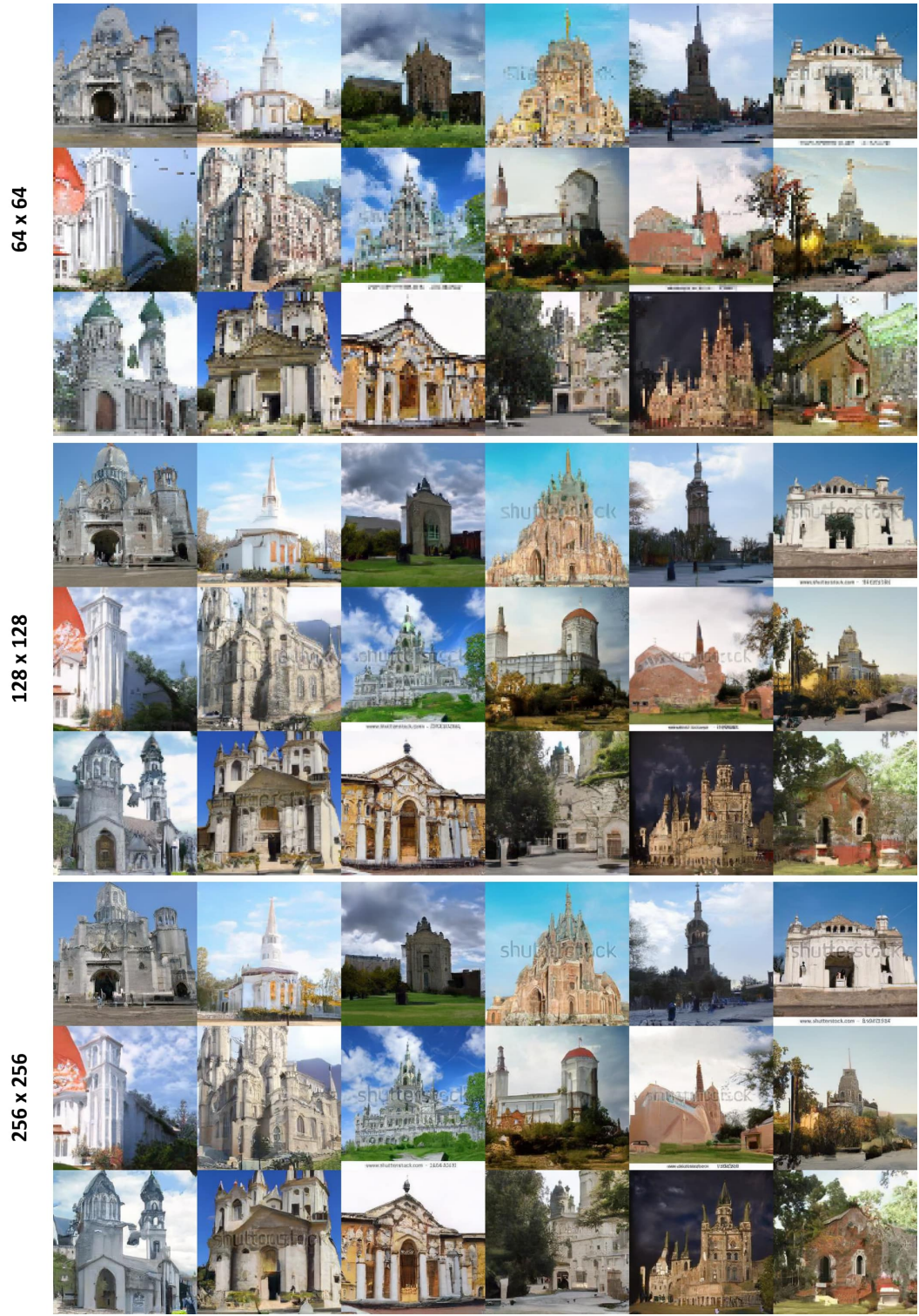


Figure 8: Additional generated images trained from LSUN-Church dataset. Resolution increases starting from top to bottom row.



Figure 9: Intermediate results of pyramidal super-resolution on FFHQ and AFHQ-dog dataset.

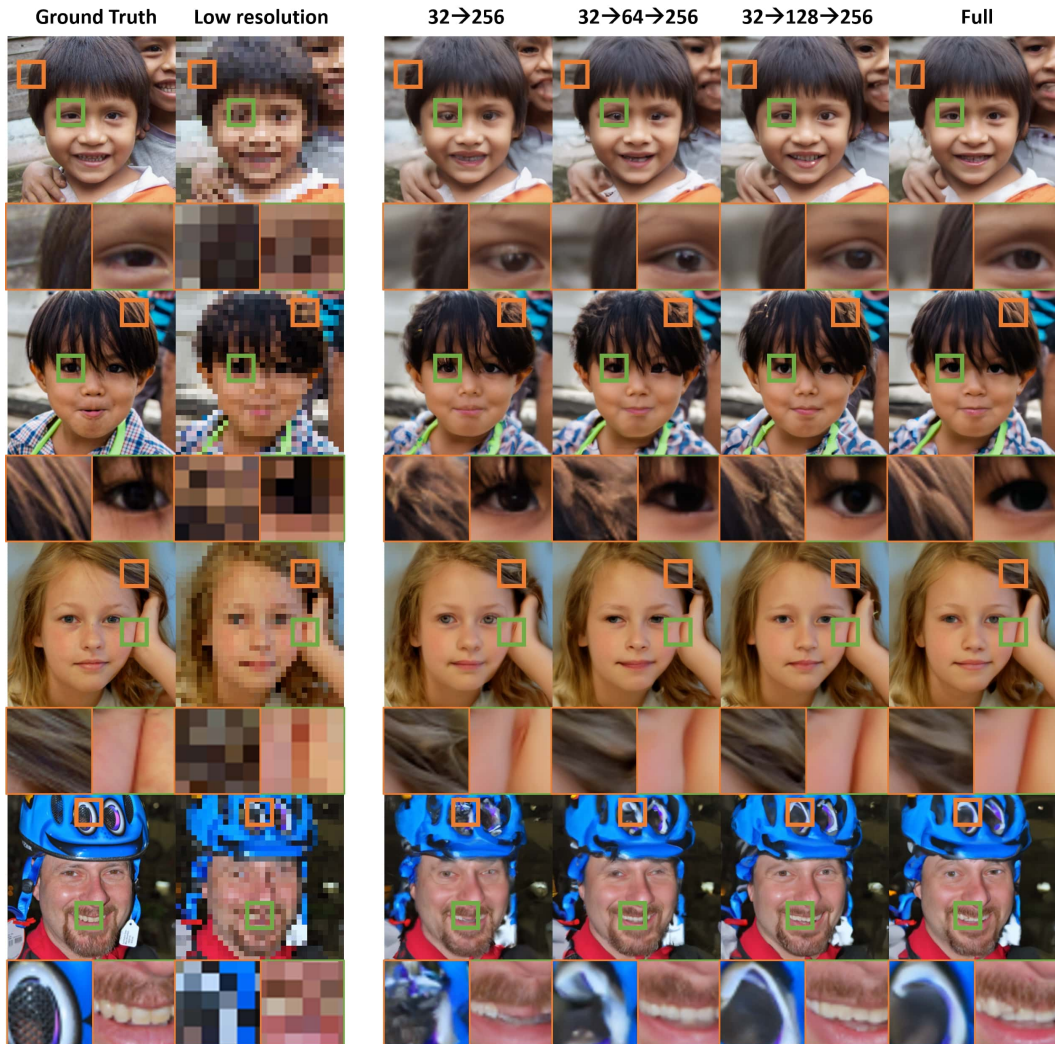


Figure 10: Visualization of the result of $\times 8$ super-resolution in Table 4 on FFHQ dataset.



Figure 11: Visualization of the result of $\times 8$ super-resolution in Table 4 on AFHQ-dog dataset.